Radial Equilibrium Example

For the purposes of this example of a radial equilibrium solution, the flow through the pump impeller is subdivided into streamtubes, as shown in figure 1, section (Mbdb). We choose to examine one generic streamtube with an inlet radius, r_1, and thickness, dr_1. Both the position, n, and the thickness, dn, of the streamtube at discharge are not known *a priori*, and must be determined as a part of the solution. Conservation of mass requires that

$$v_{m1} r_1 dr_1 = v_{m2}(n)(R_{H2} + n\cos\vartheta)dn \tag{Mbdc1}$$

where n is a coordinate measured normal to the streamlines at discharge and $n = 0$ at the hub so that $r_2 = R_{H2} + n\cos\vartheta$.

Applying the radial equilibrium assumption, the pressure distribution over the exit plane is given by

$$\frac{1}{\rho}\frac{\partial p_2}{\partial n} = \frac{v_{\theta 2}^2 \cos\vartheta}{(R_{H2} + n\cos\vartheta)} \tag{Mbdc2}$$

It is also necessary to specify the variation of the discharge blade angle, $\beta_{b2}(n)$, with position, and, for the reasons described in section (Mbdb), we choose the helical distribution given by equation (Mbbb2). Note that this implies helical blades in the case of an axial flow pump with $\vartheta = 0$, and a constant β_{b2} in the case of a centrifugal pump with $\vartheta = 90°$. Moreover, we shall assume that the flow at discharge is parallel with the blades so that $\beta_2(n) = \beta_{b2}(n)$.

The formulation of the problem is now complete, and it is a relatively straightforward matter to eliminate $p_2(n)$ from equations (Mbbg1) and (Mbdc2), and then use the velocity triangles and the continuity equation (Mbdc1) to develop a single differential equation for $v_{m2}(n)$. Assuming that the inlet is free of swirl, and that v_{m1} is a constant, this equation for $v_{m2}(n)$ can then be integrated to obtain the velocity and pressure distributions over the exit. It remains to evaluate the total energy added to the flow by summing the energies added to each of the streamtubes according to equation (Mbbc9):

$$H = \frac{1}{Q}\int_{HUB}^{TIP} \frac{(p_2^T - p_1^T)}{\rho g} 2\pi r_2 v_{m2} dn \tag{Mbdc3}$$

Nondimensionalizing the result, we finally obtain the following analytical expression for the performance:

$$\psi = \Sigma_1 + \Sigma_2\phi_2 + \Sigma_3/\phi_2 \tag{Mbdc4}$$

where Σ_1, Σ_2, and Σ_3 are geometric quantities defined by

$$\Sigma_2 = \frac{\Gamma\cot\beta_{bT2}}{\ell n\Gamma^*}\left[1 + \frac{\Gamma\sin^2\beta_{bT2}\cos^2\beta_{bT2}}{\Gamma^*\ell n\Gamma^*}\right]$$

$$\Sigma_3 = \tan^3\beta_{bT2}\left[1 - \frac{\Gamma^2\cos^4\beta_{bT2}}{\Gamma^*\{\ell n\Gamma^*\}^2}\right]$$

$$\Sigma_1 = -\Sigma_3\cot\beta_{bT2} - \Sigma_2\tan\beta_{bT2} \tag{Mbdc5}$$

where Γ and Γ^* are given by

$$\Gamma = 1 - \left(\frac{R_{H2}}{R_{T2}}\right)^2 \quad ; \quad \Gamma^* = 1 - \Gamma\cos^2\beta_{bT2} \tag{Mbdc6}$$

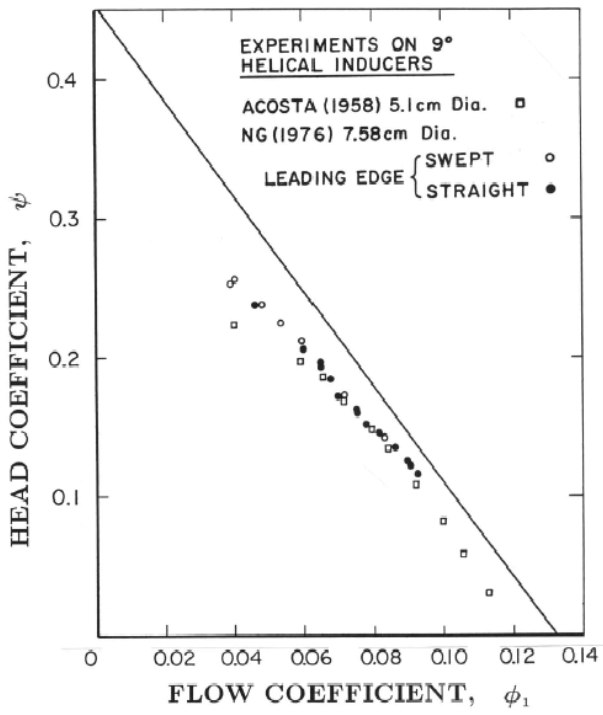

Figure 1: Non-cavitating performance of 9° helical inducers of two different sizes and with and without swept leading edges (the 7.58 *cm* inducers are Impellers III and V). Also shown is the theoretical performance prediction in the absence of losses (from Ng and Brennen 1978).

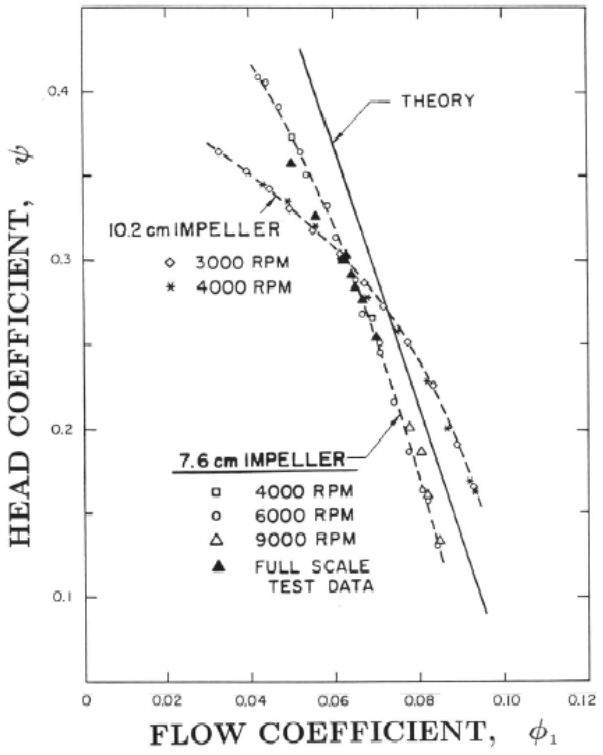

Figure 2: Non-cavitating performance of Impeller IV (7.58 *cm*, with stator) and Impeller VI (10.2 *cm*, without stator) at various rotational speeds. Also shown are full scale test data from Rocketdyne and a theoretical performance prediction (solid line) (from Ng and Brennen 1978).

Thus the geometric quantities, Σ_1, Σ_2, and Σ_3, are functions only of Γ and β_{bT2}.

Examples of these analytical performance curves are given in figures 1 and 2 and further comment on these is included in the section on inducer performance (section (????)).

Note that this idealized hydraulic performance is a function only of the geometric variables, Γ and β_{bT2}, of the discharge. Moreover, it is readily shown that in the centrifugal limit of $\Gamma \to 0$ then $\Sigma_1 \to 1$, $\Sigma_2 \to -\cot\beta_{bT2}$, $\Sigma_3 \to 0$, and the earlier result of equation (Mbbg4) is recovered.

It is of interest to explore some optimizations based on the hydraulic performance, given by equation (Mbdc4). Though the arguments presented here are quite heuristic, the results are interesting. We begin with the observation that two particular geometric factors are important in determining the viscous losses in many internal flows. If the cross-sectional area of the flow increases at more than a marginal rate, the deceleration-induced boundary layer separation and turbulence can lead to large viscous losses that might not otherwise occur. Consequently, the mean value of w_2/w_1 is an important design parameter, as implied earlier in section (Mbcd). In the present analysis, the mean value of this parameter is given by the area ratio, Ar^*, where, from geometric considerations,

$$Ar^* = \frac{\Gamma \sin\beta_{bT2}}{\cos\vartheta\,(R_{T1}/R_{T2})^2 \sin\left\{\tan^{-1}\left(\phi_2 Ar R_{T2}/R_{T1}\right)\right\}} \tag{Mbdc7}$$

We shall also use the ratio, Ar, of the area of the axisymmetric discharge surface to the area of the inlet surface given by

$$Ar = \Gamma/\cos\vartheta\,(R_{T1}/R_{T2})^2 \tag{Mbdc8}$$

In this example it is assumed that $R_{H1} = 0$; non-zero values can readily be accommodated, but do not alter the qualitative nature of the results obtained.

Many centrifugal pumps are designed with Ar^* values somewhat greater than unity because the flow must subsequently be decelerated in the diffuser and volute, and smaller values of Ar^* would imply larger diffusion losses in those nonrotating components. But, from the point of view of minimizing losses in the impeller alone, one justifiable optimization would require $Ar^* \approx 1$.

The second geometric factor that can influence the magnitude of the viscous losses in an internal flow is the amount of turning imposed on the flow. In the present analysis, we shall make use of an angle, ϵ, describing the "angle of turn" of the flow as it proceeds through the turbomachine. It is defined as the angle of the discharge relative velocity vector to the conical discharge surface minus the angle of the inlet relative velocity vector to the inlet surface:

$$\epsilon = \beta_{bT2} - \tan^{-1}\left\{\phi_2 A_r R_{T2}/R_{T1}\right\} \tag{Mbdc9}$$

Note that, in purely axial flow, the angle of turn, ϵ, is zero for the case of a flow with zero incidence through a set of helical blades of constant pitch. Also note that, in purely radial flow, the angle of turn, ϵ, is zero for the case of a flow with zero incidence through a set of logarithmic spiral blades. Therefore, using somewhat heuristic interpolation, one might argue that ϵ may be useful in the general case to describe the degree of turning applied to the flow by a combination of a nonzero incidence at inlet and the curvature of the blade passages.

For the purposes of this example, we now postulate that the major hydraulic losses encountered in the flow through the pump are minimized when ϵ is minimized. Let us assume that this minimum value of ϵ can be approximated by zero. Referring to this maximum efficiency point of operation as the "design point" (where conditions are denoted by the suffix, D), it follows from equation (Mbdc9) that

$$\phi_{2D} = \frac{R_{T1}}{R_{T2}} \frac{\tan\beta_{bT2}}{Ar} \tag{Mbdc10}$$

and hence that

$$\psi_D = \Sigma_1 + \Sigma_2\phi_{2D} + \Sigma_3/\phi_{2D} \tag{Mbdc11}$$

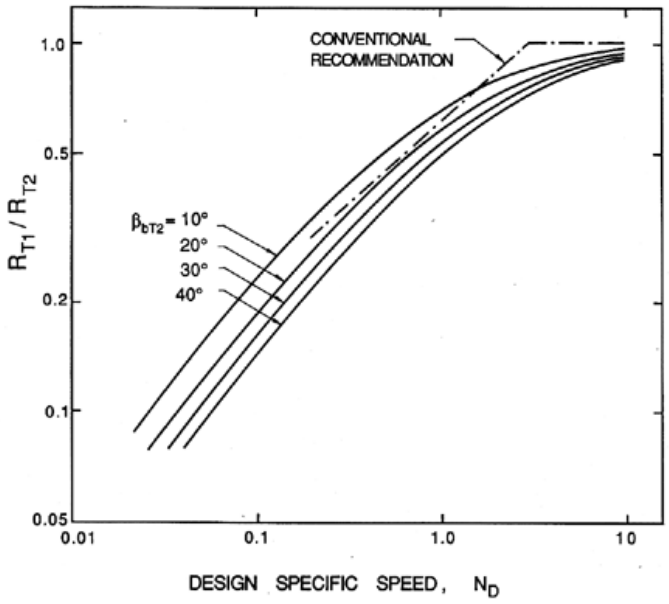

Figure 3: Comparison of the results of equation (Mbdc12) with the conventional recommendation from figure 1, section (Mbbe) for the optimum ratio of inlet to discharge tip radius as a function of design specific speed, N_D.

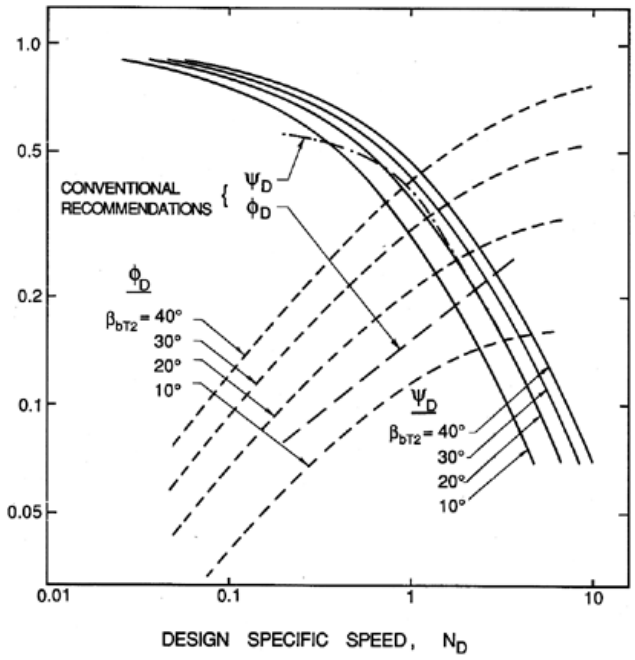

Figure 4: Comparison of the results of equations (Mbdc12) with the conventional recommendation of figure 1, section (Mbbe), for the head coefficient, ψ_D, and the flow coefficient, ϕ_D, as functions of the design specific speed, N_D.

Thus the specific speed for which the pump is designed, N_D, is given by

$$N_D = \left[\frac{\pi \tan \beta_{bT2} \left(1 - \frac{R_{H1}^2}{R_{T1}^2}\right)}{\left\{ \Sigma_1 \left(\frac{R_{T2}}{R_{T1}}\right)^2 + \frac{\Sigma_2 \tan \beta_{bT2}}{Ar} \left(\frac{R_{T2}}{R_{T1}}\right) + \frac{\Sigma_3 Ar}{\tan \beta_{bT2}} \left(\frac{R_{T2}}{R_{T1}}\right)^3 \right\}^{\frac{3}{2}}} \right]^{\frac{1}{2}} \qquad \text{(Mbdc12)}$$

and is a function only of the geometric quantities R_{T1}/R_{T2}, R_{H1}/R_{T1}, R_{H2}/R_{T2}, ϑ, and β_{bT2}.

Examine now the variation of N_D with these geometric variables, as manifest by equation (Mbdc12), bearing in mind that the practical design problem involves the reverse procedure of choosing the geometry best suited to a known specific speed. The number of geometric variables will be reduced to four by assuming $R_{H1} = 0$. Note also that, at the design point given by equation (Mbdc10), it follows that $Ar^* = Ar$ and it is more convenient to use this area ratio in place of the variable R_{H2}/R_{T2}. Thus we consider the variations of N_D with $\vartheta, \beta_{bT2}, R_{T1}/R_{T2}$, and Ar^*.

Calculations of N_D from equation (Mbdc12) show that, for specific speeds less than unity, for sensible values of Ar^* of the order of unity, and for blade angles β_{bT2} which are less than about 70° (which is the case in well-designed pumps), the results are virtually independent of the angle ϑ, a feature that simplifies the parametric variations in the results. For convenience, we choose an arbitrary value of $\vartheta = 50°$. Then typical results for $Ar^* = 1.0$ are presented in figure 3, which shows the "optimum" R_{T1}/R_{T2} for various design specific speeds, N_D, at various discharge blade angles, β_{bT2}. Considering the heuristic nature of some of the assumptions that were used in this optimization, the agreement between the results and the conventional recommendation (reproduced from figure 1, section (Mbbe)) is remarkable. It suggests that the evolution of pump designs has been driven by processes minimizing the viscous losses, and that this minimization involves the optimization of some simple geometric variables. The values of ψ_D and ϕ_D, that correspond to the results of figure 3, are plotted in figure 4. Again, the comparison of the traditional expectation and the present analysis is good, except perhaps at low specific speeds where the discrepancy may be due to the large values of Ar^* which are used in practice. Finally, we observe that one can construct sets of curves, such as those of figure 3, for other values of the area ratio, Ar^*. However, for reasonable values of β_{bT2} like 20°, the curves for $0.8 < Ar^* < 2.0$ do not differ greatly from those for $Ar^* = 1.0$.

The foregoing analysis is intended only as an example of the application of the radial equilibrium methodology, and the postscript is included because of the interesting results it produces. Clearly some of the assumptions in the postscript are approximate, and would be inappropriate in any accurate analysis of the viscous losses.